CPW Tunable Band-Stop Filter Using Hybrid Resonator and Employing RF MEMS Capacitors

Naibo Zhang, Zhongliang Deng, *Member, IEEE*, and Fan Sen

***Abstract*— This paper presents a coplanar waveguide (CPW) tunable band-stop filter using hybrid resonator and employing RF microelectromechanical systems (MEMS) capacitors. The MEMS switches are used as varactors to tune the filter resonance frequency. Defected ground structures (DGSs) with MEMS switch is employed for filter unit to achieve miniaturization of filter structure. To accurately analyze the filter unit structure parameters, a hybrid resonance circuit is used as equivalent circuit and the relationship of MEMS switch and the transverse slot capacitance is analyzed. Hereby, a CPW tunable band-stop filter, cascaded periodically by DGS and MEMS switches, is fabricated on a glass substrate ($\varepsilon_r = 3.78$, tan $\delta = 0.0012$). The filter has a midband retune loss of 2.3–2.8 dB and a tuning range of 35% from 8.5 to 12.3 GHz with a maximum dc voltage of 44 V. Finally, we propose a solution to achieve constant bandwidth when center frequency changes.**

***Index Terms*— Coplanar waveguide (CPW), defected ground structure (DGS), RF microelectromechanical systems (MEMS), tunable band-stop filter.**

I. Introduction

In the modern planar microwave system, periodic structures have recently attracted much attention in the microwave and millimeter-wave community [1]. The Photonic Bandgap in [2] and the defected ground structure (DGS) in [3] and [4] are typical periodic structures proposed previously for microstrip line. However, they are neither uniplanar nor truly 1-D structures since their defected ground planes are on the back side of substrate. Periodic structures for coplanar waveguide (CPW) can be realized on the same plane, because it is real uniplanar, 1-D structure [5]. Lim *et al.* [5] presented a spiral-shaped DGS for CPW [5], and Amr*et al.* [6], Karim*et al.* [1], [8], and Muhammad *et al.* [7], proposed types of DGS with dumbbell-shaped CPW. Moreover, most reports just proposed a performance, rarely considered the design method and structural modeling process.

In addition to the periodic structures of CPW, much effort has also been made to introduce tunable filter using microelectromechanical systems (MEMS) switch. The development of tunable filters is of great commercial and military interest. The filters substantially reduce the size of the analog front-end subsystem for multiband applications and can be used to dynamically reject large signal interferers. In recent years, many tunable filters using MEMS technology are reported, including digital tunable filter [9]–[11] and analog tunable filter [12]–[16]. The analog filter provides potential advantages of low cost, small size, and inherent compatibility with microwave circuitry. Yet the adjustable range is limited in most reports, for instance, the tuning range in [17]–[21], is 4.2%, 9%, 10%, 14%, and 15%, respectively. Montserrat Fernandez–Bolanos *et al.* proposed a tunable band-stop filter with tuning range of 55% and low dc bias voltage [22], Siamak Fouladi *et al.* presented a tunable band pass filter with tuning range of 127% and a maximum dc voltage of 6 V [23], Nevertheless, the shape factor of the filter is not good enough.

We previously reported a tunable band-stop filter [24]. In this paper, a band-stop filter with periodic CPW structures and MEMS switches is presented. The hybrid resonator circuit, consisted by shunt and series resonator circuits, is analyzed and designed as equivalent circuit. The lower resonance frequency has been achieved by combining the shunt and series resonator. As a result, when the resonance frequency is specified, the filter unit size with MEMS switch is smaller than the unit without it. To demonstrate the relationship of MEMS switch and transverse slot capacitance, the parameter λ was introduced. The switch structures are analyzed to tune the resonance frequency of band-stop filter. We achieved an acceptable agreement between measured and simulation results. A tuning range of 35% with the center frequency from 8.8 to 12.3 GHz is presented, while dc voltage is tuned from 0 to 44 V.

This paper is organized as follows. Section II describes the filter unit, the equivalent circuit, and the unit structure parameters. In Section III, the MEMS switch structure is designed and analyzed. The tunable band-stop filter and equivalent circuit are presented in Section IV, including fabrication, simulation/measurement results, and bandwidth of the filter. Finally, the conclusion is presented in Section V.

II. Unit Structure Modification and Analysis

A. Unit Structure Analyses

The dumbbell-shaped DGS and two wing-shaped DGS were initially presented in [21] and [22], which have symmetrical structures with respect to the center line. Fig. 1(a) shows two wings with four slot-shaped DGS, as in [4] and [6]. Designing

Manuscript received May 23, 2012; revised January 16, 2013, March 28, 2013, and May 21, 2013; accepted June 14, 2013. Date of current version July 19, 2013. This work was supported in part by the Foundation of National Key Laboratory of Science and Technology on Micro/Nano Fabrication. The review of this paper was arranged by Editor A. M. Ionescu.

N. Zhang is with the Beijing R & D Center, The Fifty-Fourth Research Institute of China Electronic Technology Group Corporation (CETC-54), Beijing 100070, China (e-mail:zhangnaibai@163.com).

Z. Deng and F. Sen are with the School of Electronic Engineering, Beijing University of Posts and Telecommunications, Beijing 100876, China (e-mail: dengzhl@bupt.edu.cn; 17217934@qq.com).

Color versions of one or more of the figures in this paper are available online at http://ieeexplore.ieee.org.

Digital Object Identifier 10.1109/TED.2013.2270359

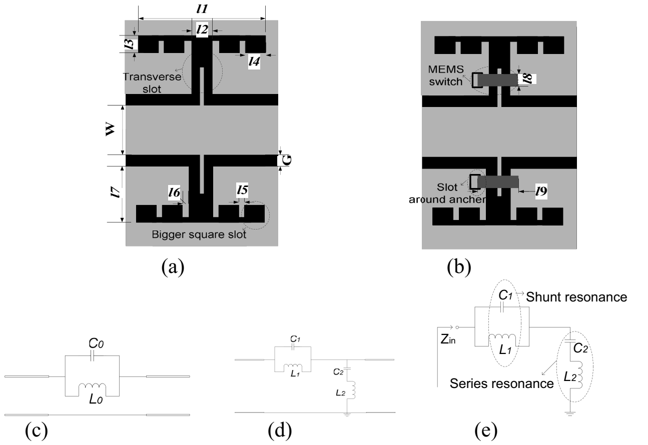

Fig. 1. (a) Two wings with four slot-shaped DGSs. (b) Schematic of unit cell structure. (c) Equivalent circuit model for Fig. 1(a). (d) Equivalent circuit model for Fig. 1(b). (e) Hybrid resonator circuit.

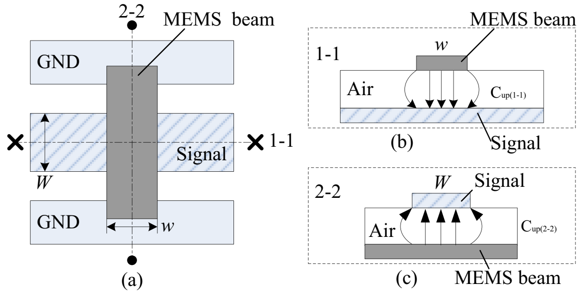

Fig. 2. MEMS switch. (a) Top view model of MEMS switch. (b) Side view of MEMS switch from side "1−1." (c) Side view of MEMS switch from side "2−2."

the parameters needed, i.e.: 1) the slot size l_2; 2) the square slot, $l_3 \times l_4$; and 3) the length of transverse slot, l_7. Ignoring the resistance, an equivalent parallel $L-C$ circuit in Fig. 1(c) is equivalent to Fig. 1(a) structure. C_0 is mainly contributed by the transverse slot on the ground, and L_0 is related to the magnetic flux passing through the apertures on the ground [1], [24].

The hybrid resonator with series and shunt resonators was first presented in [25] based on microstrip line. In this paper, the unit structure with two MEMS switches in Fig. 1(b) equivalent to the hybrid resonator in Fig. 1(d). The MEMS switch in Fig. 1(b) is equivalent to series resonator. In Fig. 1(d), C_1 is mainly contributed by the transverse slot and switch, L_1 is related to the magnetic flux passing through the apertures on the ground, and $C_1 = \lambda C_0$, $L_1 = L_0$. As the parameter λ is affected by switch height, while the capacitance C_1 is determined by λ, the capacitance C_0 is decided by transverse slot size. Inductances L_0 and L_1 are determined by the apertures on the ground. Capacitance C_2 is mainly contributed by several factors, such as switch beam size, the bottom electrode size, and the MEMS switch height. Inductance L_2 is contributed by the switch beam, the anchor of MEMS switch, and the slot around anchor.

B. Circuit Analyses and the Unit Structure Parameters Design

To determine the parameters of the unit structure in Fig. 1(b), the resonator frequency and the unit equivalent circuit must be analyzed [25], [26]. Fig. 1(e) shows the hybrid resonant circuit, which consists of series resonator circuit and shunt resonator circuit. The impedance Z_{in}, can be given

$$\begin{aligned} Z_{\text{in}} &= j\frac{w^4L_1L_2C_1C_2 - w^2(L_1C_2 + L_1C_1 + L_2C_1) + 1}{wC_2(w^2C_1L_1 - 1)} \\ &= j\frac{w^4 - w^2(w_1^2 + w_2^2 + w_3^2) + w_1^2w_2^2}{w^2w_2^2C_2(w^2 - w_1^2)} \end{aligned} \tag{1}$$

where w_1 is the resonance frequency of shunt resonator $L_1 - C_1$, w_2 is the resonance frequency of shunt resonator $L_2 - C_2$, and w_3 is the resonance frequency of shunt resonator $L_1 - C_2$. The resonance frequencies are calculated when $Z_{\text{in}} = 0$ in (1). There are four roots when $Z_{\text{in}} = 0$, two of roots are positive and the rest are negative. We define w_{R1} and w_{R2} are two positive roots of $Z_{\text{in}} = 0$. The parameters L_1, L_2, C_1, can be expressed by C_2, w_1, w_2, w_{R1}, w_{R2}, where C_2 is the capacitance between switch beam and bottom electrode, containing two parts, the main capacitance C_{ud} and fringing capacitance C_f. The capacitance C_2 is calculated by microstrip characteristic impedance. The MEMS switch is equivalent to microstrip transmission line as shown in Fig. 2.

As the width of MEMS switch l_8 is much bigger than d_4, the microstrip characteristic impedance offered by Wheeler

$$Z_0 = \frac{120\pi}{\sqrt{\varepsilon_e}\,[W/d_4 + 1.393 + 0.667\ln(W/d_4 + 1.444)]} \tag{2}$$

where W is the width of up electrode, ε_e is the equivalent dielectric constant of microstrip. The microstrip characteristic impedance is also represented as the following:

$$Z_0 = \frac{1}{\nu C_2} \tag{3}$$

where ν is the speed of microwave in air.

As the fringing capacitance Cf is composed of fringing capacitance of MEMS beam (C_{f1}) and fringing capacitance of signal line (C_{f2}), C_f equals to $C_{f1} + C_{f2}$, the whole capacitance C_2 equals to $C_{\text{ud}} + C_{f1} + C_{f2}$, where C_{ud} is the main capacitance.

$$\begin{aligned} C_f &= C_2 - C_{\text{ud}} \\ &= \frac{\sqrt{\varepsilon e}\,[W/d_4 + 1.393 + 0.667\ln(W/d_4 + 1.444)] + \sqrt{\varepsilon e}\left[w/d_4 + 1.393 + 0.667\ln(w/d_4 + 1.444)\right]}{120\pi\nu} \\ &\quad -\frac{1}{2k\pi}\frac{\varepsilon_{\text{eff}}S_2}{d_1} \end{aligned} \tag{7}$$

TABLE I
PARAMETERS OF THE CIRCUIT

Parameters			C_1(pF)	L_1(nH)	C_2(pF)	L_2(nH)
			0.21	0.7	0.0151	0.398
C_0 (pF)	L_0 (nH)	f_0 (GHz)	f_1 (GHz)	f_2 (GHz)	f_{R1} (GHz)	f_{R2} (GHz)
0.13	0.7	16.5	13.5	65	13	67.5

TABLE II
PARAMETERS OF THE UNIT STRUCTURE

Parameters (μm)	The width of unit l_1	Slot size l_2	The square slot size l_3, l_4	The distance between square slots l_5
	1700	75	390	40
	The distance between square slot and transverse slot l_6	Beam width l_8	Beam length l_9	W/G
	30	130	280	200/22
	The distance between anchor and transverse slot l_{11}		The slot size below switch beam l_{12}	
	102.5		25	

The $C_{\text{up}}(1-1)$ is composed of C_{f1} and C_{ud}, while $C_{\text{up}}(2-2)$ is composed of C_{f2} and C_{ud}. From (2) and (3), the capacitances are given as

$$C_{\text{up}(1-1)} = C_{\text{ud}} + C_{f1} = \frac{1}{\upsilon Z_{0(1-1)}}$$
$$C_{\text{up}(2-2)} = C_{\text{ud}} + C_{f2} = \frac{1}{\upsilon Z_{0(2-2)}}. \quad (4)$$

The main capacitance C_{ud} is expressed as

$$C_{\text{ud}} = \frac{1}{4k\pi}\frac{\varepsilon_{\text{eff}} S_2}{d_1}. \quad (5)$$

Then the capacitance C2 is calculated by (2)–(5) as follows:

$$C_2 = C_{\text{ud}} + C_{f1} + C_{f2} = C_{\text{up}(1-1)} + C_{\text{up}(2-2)} - C_{\text{ud}}. \quad (6)$$

Then the fringing capacitance C_f is shown in (7) at the bottom of the previous page.

The parameter $S_2 (S_2 = l_8 \times l_{10})$ is the area determined by switch beam width l_8 and bottom electrode length l_{10}, d_4 is the distance between switch beam and bottom electrode, and k is the air permittivity. The up-state fringing capacitance for MEMS shunt capacitive switches range from $0.2C_2$ to $0.4C_2$ for most switches, the down-state fringing capacitance reduces to $0.05C_2$ [12], so C_f range from $0.05C_2$ to $0.4C_2$ as MEMS switch height changed. When MEMS switch is down state, the fringing capacitance C_f can be neglected, when up state, the fringing capacitance is about $0.25C_2$.

To give an example, the bottom electrode width is defined (20 μm), the width of switch beam l_8 is 130 μm, f_1, f_2, and f_3 are 13.5, 65, and 15 GHz, respectively, the parameters of the hybrid circuit are set in Table I.

The unit structure discussed in this paper is implemented on a substrate (quartz) of 425 μm with a dielectric constant of 3.78 and tanδ of 0.0012. To design parameters of the unit, we referred to [24] and [27] and simulated in an electromagnetic (EM) simulator (ADS-Momentum), dimensions of unit structure are given in Table II.

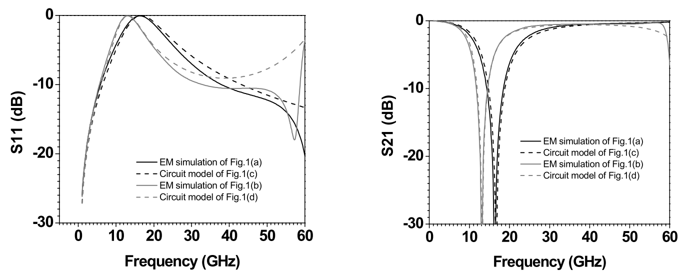

(a) (b)

Fig. 3. Comparison of parameter extraction and EM simulation results of the filter unit structures. (a) Return loss. (b) Insertion loss.

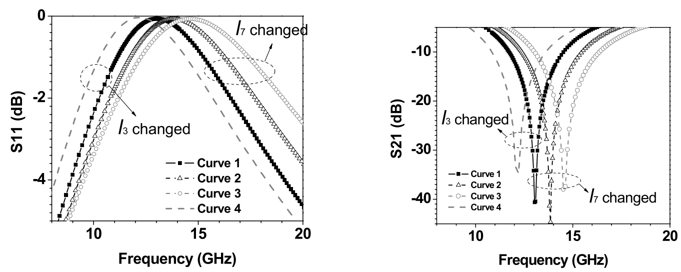

(a) (b)

Fig. 4. Performances effect by slot sizes. (a) Return loss. (b) Insertion loss.

Fig. 3 shows the comparison results from extraction circuit simulation and structure simulation. The structure simulation result shows a good agreement with extraction circuit simulation result. The performance illustrates that when the resonance frequency is determined, the resonator size could be reduced and capacitance C_0 could be affected by MEMS switch.

C. Effect of Slot Sizes l_3, l_7

The size l_7 relates to the parameter C_1, if dimension l_7 changes, the resonance frequency f_{R1} could be tuned. In Fig. 4, it shows that the resonance frequency increases from 13 to 15 GHz, as dimension l_7 decreases from 1280 to 880 μm.

The dimension l_3 affects inductance (L_1). Fig. 4 shows when l_3 is 390 μm, the resonance frequency is 13 GHz (curve 1), when l_3 is 590 μm, the resonance frequency is 12 GHz (curve 4).

D. Effect of MEMS Switch Height d_1

As shown in (5)–(6), capacitance C_2 is determined by d_1. The transverse slot in Fig. 1(a) determines capacitance C_0, while the value ΔC_1 is mainly contributed by the parameter λ when other sizes are specified.

Fig. 5(a) and (b) show that the center frequency is altered 2.5 GHz as the MEMS switch height d_1 increase from 0.1 to 1 μm.

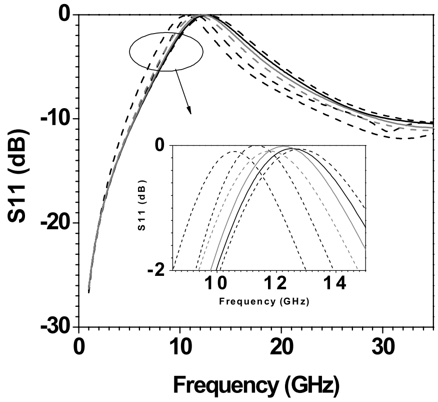

(a)

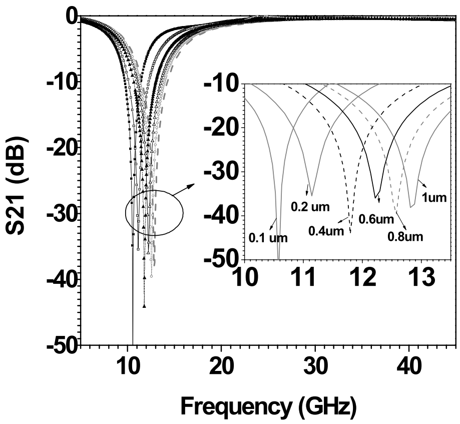

(b)

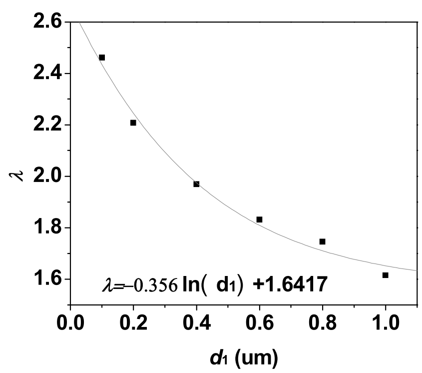

(c)

Fig. 5. Simulation results for tuning MEMS switch height d_1. (a) Return loss. (b) Insertion loss. (c) Relationship between λ and d_1.

As other parameters of MEMS switch are specified, parameter λ is determined by MEMS switch height d_1. Fig. 5(c) shows the value of λ when d_1 tune from 1 to 0.1 μm. As $C_1 = \lambda C_0$, $L_1 = L_0$, C_0, and L_0 are fixed, the frequency (f_1) changes in nonlinear, which is determined by parameter λ in (8)–(9), and (8) is obtained by numerical fitting. Fig. 4(b) shows that the peaks rejection values are not linear with the height of MEMS switch

$$\lambda = -0.356 ln\,(d_1) + 1.6417 \tag{8}$$

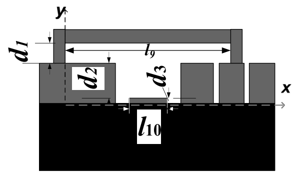

(a)

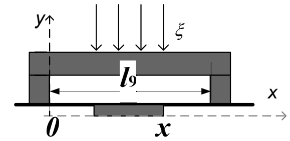

(b)

Fig. 6. (a) Side view of MEMS switch. (b) Mechanics model of MEMS switch.

$$f_1 = \frac{1}{2\pi\sqrt{L_1 C_1}} = \frac{1}{\sqrt{\lambda}}\frac{1}{2\pi\sqrt{L_0 C_0}}. \tag{9}$$

III. MEMS Switch Analysis

To avoid the "pull-down" and instability of the MEMS switch, the specially switch structure is designed as Fig. 6(a). The height of switch is d_1, the distance between switch beam and low electrode is $d_4 = d_1 + d_2$. The thickness of bottom electrode is d_3. As the position of switch beam decreases to (2/3)d_4, the increase of electrostatic force is greater than the increase of restoring force, resulting in two cases: 1) the beam position becoming unstable and 2) collapse of the beam to the down-state position [12]. To avoid the cases above, we design $d_1 = (1/2)d_2$; the distance d_1 can be accurately controlled by dc voltage. When the beam's position reaches to (2/3)d_4, the switch beam could touch the ground, avoiding the "pull-down" and instability of the switch. The dc voltage is $\mathrm{V} = d_4(2k^{\triangle}d/(\varepsilon\varepsilon_0 S_2))^{1/2}$ [12], $\varepsilon = 8.85 \times 10^{12}$F/m, $\varepsilon = 1$, $^{\triangle}d$ is the displacement of switch beam, S_2 is the area of electrodes, and k is the spring constant.

The MEMS switch is symmetrical about bottom electrode the mechanics model is built in Fig. 6(b). The electrostatic force loaded on the middle part of beam is from $(l_9 - x)$ to x, and the whole size of beam is l_9. ξ represents the load per unit area. The spring constant for the MEMS switch is modeled in two parts. One part, k_1, is due to the stiffness of the bridge, which accounts for the material characteristics such as Young's modulus [28], E (Pa), and the moment of inertia, I (m^4) $= l_9 t^2/12$, t is the thickness of switch beam. The other part of the spring constant, k_2, is due to the biaxial residual stress, $S'(\mathrm{Pa}) = \sigma(1 - \nu)l_9 t$, ($\nu$ is the Poisson's ratio) [12].

Holes in beam's surface are designed to etch photoresisit below the beam, which will bring spring constant error. The effect of holes needs to be considered; the holes release some of the residual stress in the beam and reduce the Young's modulus of the MEMS structure [29]. The reduction of the residual stress is equivalent to $\sigma = (1 - \mu)\sigma$, where σ is the residual stress with no holes. The spring constant is revised to $k = \lambda_1(k_1 + k_2)$, $(0 < \lambda_1 < 1)$, and the parameters in this paper λ_1 σ, E, t, and k are about 0.78, 64 MPa [30], 53 GPa [30], 1 μm, and 6.8 N/m, respectively. The sizes of MEMS switches are designed to the tunable band-stop filter, and the dimensions l_8, l_9, l_{10}, d_1, d_2, d_3, and S_2, are 130, 280 μm, 22 μm, 1 μm, 2 μm, 0.2 μm and (130 × 22) μm^2, respectively.

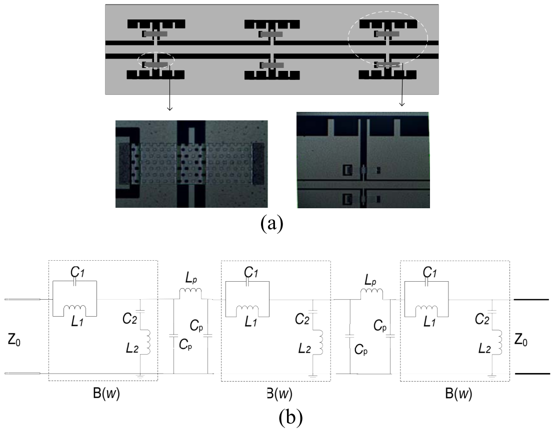

Fig. 7. (a) Fabricated tunable band-stop filter. (b) Equivalent circuit of the filter.

IV. Measurement Results and Discussions

A. Fabrication and Measurement

In this section, the fabrication and measurement of the filter will be described.

To demonstrate the validity of equivalent circuit and extracted parameters for the proposed DGS unit section, the filter is cascaded by three unit resonator structures as in [1], [4], [7], and [31]. Fig. 7 shows the three-pole band-stop filter, the fabricated MEMS switch, unit resonator structure, and equivalent circuit. The lumped band-stop filter circuit can be easily obtained from the equivalent circuit of unit structure by proper frequency and impedance scaling [4]. The dc voltage is loaded between signal and ground, since bottom electrode of MEMS switch connects to signal line. One anchor of MEMS switch connects to ground, and the other connects to the region around by slot. If dc voltage continues changing, center frequency will change in accordance.

The fabrication is made in the Institute of Microelectronics in Peking University. The surface micromachining technology is used for fabrication [7], [32]–[35], and low-temperature process is used to implement MEMS switch's fabrication. Substrate is glass, metal layer is aluminum, and photoresist is used to be the sacrifice layer.

By measurement, the holes size on the switch surface is about 3.5 × 3.5–4.2 × 4.2 μm^2, the distance between two holes center is about 8.5–10 μm. The dimensions d_1, d_2, and d_3 are 1.07, 2.18, and 0.21 μm, respectively. The surface is a little bit uneven within the scope of allowable error. Agilent E8363B vector network analyzer is used to measure the S (S_{21}, S_{11}) parameters of the filter. All experiments are performed in the room environment without any packaging.

The comparison between simulation and measurement shows an acceptable agreement in Fig. 8. It has a retune loss of −2.3 dB at 12.3 GHz and −3 dB bandwidth of 4.5 GHz without dc bias. When 44 V is loaded, the filter shows a retune loss of −2.8 dB at 8.5 GHz and −3 dB bandwidth of 2.1 GHz. Fig. 9 shows S_{11}/S_{21} for different values of dc bias voltage. The corresponding data are summarized in Table III.

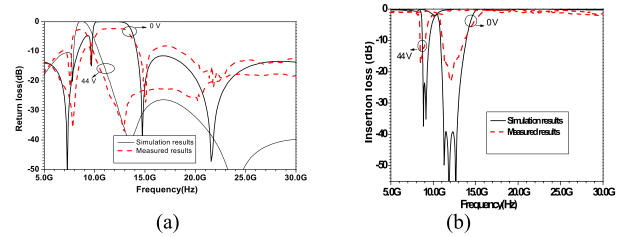

Fig. 8. (a) Return loss of tunable filter. (b) Insertion loss of tunable filter.

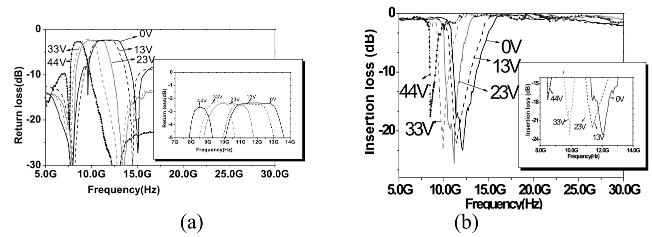

Fig. 9. Response of the tunable filter for different values of dc voltages.

TABLE III
Measured Parameters of the Tunable Filter for Different Values of Bias Voltage

Bias voltage(V)	0	13	23	33	44
Center frequency (GHz)	12.3	11.8	11.2	9.8	8.5
Band width -3dB (GHz)	4	3.5	3.1	2.6	2.1
Retune loss(dB)	2.3	2.4	2.5	2.6	2.8

B. Discussions and Improvements

From Fig. 8, the simulation results and measurement results are not match accurately, the reasons are given as follow.

Because the fringing fields that "fill" the area of the beam holes, when the diameter of the holes is less than 3∼4 d_1 [12], the effect of the holes can be negligible when MEMS switch is up state. In this paper, the hole size is designed as 3 × 3 (μm^2), but because the geometrical factors for the foundry process, the measurement results is about 3.5 × 3.5–4.2 × 4.2 (μm^2), which affect capacitance and inductance of MEMS switch, and the performances of filter will be affected, therefore, the comparison between simulation and measurement results does not show a good agreement.

When the frequency is greater than 26 GHz, Fig. 8(a) shows the rejection factor (insertion loss) of one curve is only −20 dB when it should have been −40 dB, which is due to the test error, fabrication error, and the material loss of the filter. The main error is caused by test. For instance, the guide wave line was affected outside, which will change performance of high frequency easily, and the probe did not plunge into metal layer deeply enough, which will also change the filter performance. All experiments test environment (without any packaging, bring less than 1 dB loss) and the effect of geometrical factors for the foundry process (MEMS fabrication error). The metal material (Al) is set as perfect electro-conductivity in momentum simulator, which will lead to less than 1 dB loss. All of those affected

TABLE IV
MEASURED PARAMETERS OF THE TUNABLE FILTER FOR DIFFERENT VALUES OF BIAS VOLTAGE

Parameters (μm)	l_1	l_2	$l_{3,}l_4$	l_5
	1825	50	400	50
	l_6	l_8	l_9	W/G
	45	130	380	200/22
	The length of transverse slot l_7		The distance between anchor and transverse slot l_{13}	
	1280		270	

the absolute value of capacitance, which would change the resonance frequency and affect the rejection of performance.

Fig. 9 shows when tuning the switch height (d_1), the bandwidth of the filter changes. It has a retune loss of −2.5 dB at 11.5 GHz and −3 dB bandwidth of 3 GHz with 13 V dc voltage. When 23 V is loaded, the filter shows a retune loss of −2.4 dB at 11.2 GHz and −3 dB bandwidth of 3.1 GHz. When 33 V is loaded, the filter shows a retune loss of −2.6 dB at 9.8 GHz and −3 dB bandwidth of 2.6 GHz. An analytic improved approach is given in the following.

Fig. 7(b) shows the equivalent circuit [36]. The input impedance is expressed as

$$\begin{aligned} Z &= 3(jwC_1 + \frac{1}{jwL_1})^{-1} \\ &\quad +2\left[\left(jwL_2 + \frac{1}{jwC_2}\right)^{-1} + jwC_p\right]^{-1} \\ &\quad +2jwC_p + 2jwL_p. \end{aligned} \tag{10}$$

The −3 dB cut-off angular frequency (w_{c1}, w_{c2}) can be determined as shown in (11) at the bottom of this page.

The bandwidth (BW) of filter is approximately as shown in (12) at the bottom of this page, where the $f(L_P, C_P)$ is the polynomial of L_P and C_P, and $f(L_P, C_P)$ is a determined data. When MEMS switch height is reduced, the dates L_2, C_2, and C_1 increase, L_1, L_p, and C_P keep constant, the value of $(1/L_1{+}1/L_2)^{0.5}[1{-}(C_1C_2)^{0.5}]/(C_1 + C_2)^{0.5}$ decreases, and the value of $[L_PL_2C_2^3(C_1 + L_1)]^{0.5}/[L_1C_PC_1^3(C_2 + L_1)]^{0.5}$ increases. But the value of whole function (17) is decreasing, so the bandwidth BW decreases. The filter performance shows the bandwidth decreases when the dc bias increases.

To keep bandwidth (BW) constant, the structure of MEMS switch is designed as in Fig. 10(b) and the parameters of the tunable filter are adjusted by structure optimization as Table IV. The structure in Fig. 10(a) is a symmetrical clamped MEMS switch [37], while Fig. 10(b) shows cantilever MEMS switch, the width (l_8) and length (l_9) of MEMS switch is changed to 130 and 380 μm in order to increase L_2 and C_2. When the switch height (d_1) decreases, the value of $[L_2C_PC_2^3(C_1 + L_1)]^{0.5}/[L_1L_PC_1^3(C_2 + L_1)]^{0.5}$ will increase faster than before, which could make the bandwidth (BW) keeping constant as much as possible.

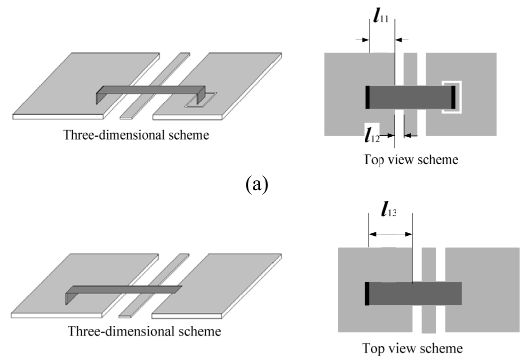

Fig. 10. MEMS switch structure. (a) MEMS switch in Fig. 9. (b) Revised MEMS switch.

TABLE V
PARAMETERS OF THE UNIT STRUCTURE

Parameters (μm)	l_1	l_2	$l_{3,}l_4$	l_5
	1825	50	400	50
	l_6	l_8	l_9	W/G
	45	130	380	200/22
	The length of transverse slot l_7		The distance between anchor and transverse slot l_{13}	
	1280		270	

The improved filter is only simulated without fabrication. Fig. 11 shows simulation results of the improved tunable band-stop filter. When MEMS switch height (d_1) is changed from 1.2 to 0.15 μm, the bandwidth (at −3 dB) change from 8.7 to 8.3 GHz, and Fig. 11 shows parameters S_{11}/S_{21} for different values of the switch height (d_1). The corresponding data are summarized in Table V.

The performances in Fig. 8 have two peaks of rejection rather than a single one; the reasons are as below.

The return loss is given by [1], and is shown in (13) at the top of next page.

When S_{11} is equal to 0 in (18) and frequency is less than 30 GHz, leading to three pole points, which means the

$$|S_{21}| = \left|\frac{2Z_0}{2Z_0 + Z}\right| = \frac{2Z_0}{\sqrt{4Z_0^2 + \left\{3(jwC_1 + \frac{1}{jwL_1})^{-1} + 2\left[(jwL_2 + \frac{1}{jwC_2})^{-1} + jwC_p\right]^{-1} + 2jwC_p + 2jwL_p\right\}^2}} = \frac{1}{\sqrt{2}} \tag{11}$$

$$BW = |w_{c1} - w_{c2}|/2\pi \approx \left|\frac{f(L_P, C_P)}{2\pi}\sqrt{\frac{1}{L_1} + \frac{1}{L_2}}\frac{1 - \sqrt{C_1C_2}}{\sqrt{C_1 + C_2}}\frac{\sqrt{L_2C_PC_2^3(C_1 + L_1)}}{\sqrt{L_1L_PC_1^3(C_2 + L_1)}}\right| \tag{12}$$

$$\begin{aligned}\frac{d|S_{11}|}{dw} &= \frac{d|\frac{Z}{2Z_0+Z}|}{dw}\\ &= d\left(\frac{|3(jwC_1+\frac{1}{jwL_1})^{-1}+2\left[(jwL_2+\frac{1}{jwC_2})^{-1}+jwC_p\right]^{-1}+2jwC_p+2jwL_p|}{\sqrt{4Z_0^2+\left\{3(jwC_1+\frac{1}{jwL_1})^{-1}+2\left[(jwL_2+\frac{1}{jwC_2})^{-1}+jwC_p\right]^{-1}+2jwC_p+2jwL_p\right\}^2}}\right)\Big/dw=0\end{aligned} \tag{13}$$

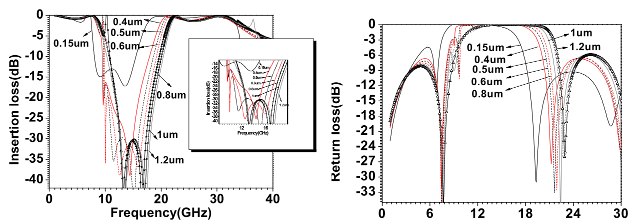

(a) (b)

Fig. 11. (a) Insertion loss of tunable filter. (b) Return loss of tunable filter.

TABLE VI
SIMULATION PARAMETERS OF THE TUNABLE FILTER FOR DIFFERENT VALUES OF BRIDGE HEIGHT

Bridge height(μm)	0.15	0.4	0.5	0.6	0.8	1.0	1.2
Center frequency (GHz)	11.2	13	13.5	14.2	15	15.3	15.5
Band width -3dB (GHz)	8.3	8.5	8.6	8.6	8.7	8.7	8.7

performance of filter has two peaks of rejection rather than a single one. Fig. 8(a) shows two peaks of rejection rather than a single one as the results in [1] and [38].

V. CONCLUSION

The resonator unit was analyzed, the equivalent circuits were modeled for the unit, and the performances showed a good agreement between structure simulation and circuit simulation. The parameter λ was used to analyze the capacitance C_1 and MEMS switch height (d_1). An analytical process was presented to design the MEMS switch structure for the MEMS switch. Then the tunable band-stop filter was designed, fabricated, and measured; the performances of the filter showed that the tuning range of the filter was about 35%, and the experiment showed an acceptable agreement between measured result and simulation results with the center frequency from 8.8 to 12.3 GHz. In addition, an analytic approach for the filter design made it possible to achieve a constant bandwidth when tuning the MEMS switch height.

APPENDIX

In Section II, some deductions are given as following.

In (1), where w_1, is the resonance frequency of shunt resonator $L_1 - C_1$, w_2, is the resonance frequency of shunt resonator $L_2 - C_2$, w_3, is the resonance frequency of shunt resonator $L_1 - C_2$

$$\begin{aligned} w_1 &= 2\pi f_1 = \frac{1}{\sqrt{L_1C_1}}\\ w_2 &= 2\pi f_2 = \frac{1}{\sqrt{L_2C_2}}\\ w_3 &= \frac{1}{\sqrt{L_1C_2}}. \end{aligned} \tag{14}$$

The resonance frequencies are calculated when $Z_{\text{in}} = 0$ in (1), and then the value of resonances is given by

$$w^2 = \frac{(w_1^2+w_2^2+w_3^2) \pm \sqrt{(w_1^2+w_2^2+w_3^2)^2 - 4w_1^2w_2^2}}{2}. \tag{15}$$

There are four roots when $Z_{\text{in}} = 0$. From (15), two of roots are positive and the rest are negative, and we define w_{R1} and w_{R2} are two positive roots of $Z_{\text{in}} = 0$; the following conditions can be satisfied:

$$w_{R1}^2.w_{R2}^2 = w_1^2.w_2^2 w_{R1}^2 + w_{R2}^2 = w_1^2 + w_2^2 + w_3^2. \tag{16}$$

It will obtain the following:

$$\begin{aligned} w_{R1}^2 &= \frac{w_1^2.w_2^2}{w_{R2}^2},\\ w_3^2 &= w_{R1}^2 + w_{R2}^2 - w_1^2 - w_2^2,\\ &= \frac{(w_{R1}^2+w_{R2}^2).w_1^2 - w_1^4 - w_{R1}^2.w_{R2}^2}{w_1^2}. \end{aligned} \tag{17}$$

The parameters L_1, L_2, C_1, can be expressed by C_2, w_1, w_2, w_{R1}, w_{R2}, using (14), (16), and (17)

$$\begin{aligned} L_1 &= w_3^2\\ C_2 &= \frac{\left((w_{R1}^2+w_{R2}^2)w_1^2 - w_1^4 - w_1^2w_2^2\right)C_2}{w_1^2}\\ L_2 &= \frac{1}{w_2^2C_2}\\ C_1 &= \frac{1}{\left((w_{R1}^2+w_{R2}^2)w_1^2 - w_1^4 - w_1^2w_2^2\right)C_2} \end{aligned} \tag{18}$$

where C_2 is the capacitance between switch beam and bottom electrode, containing two parts, the mainly capacitance C_{ud} and fringing capacitance C_f.

ACKNOWLEDGMENT

The authors would like to thank Prof. Z. Jinwen and Y. Zhaohui for their technical discussions, and Dr. J. Lin and C. Fang for their language support.

REFERENCES

[1] M. F. Karim, A.-Q. Liu, A. Alphones, X. J. Zhang, and A. B. Yu, "CPW band-stop filter using unloaded and loaded EBG structures," *IEE Proc. Microw. Antennas Propag.*, vol. 152, no. 6, pp. 434–440, Dec. 2005.

[2] V. Radisic, Y. Qian, R. Coccioli, and T. Itoh, "Novel 2-D photonic bandgap structure for microstrip lines," *IEEE Microw. Guided Wave Lett.*, vol. 8, no. 2, pp. 69–71, Feb. 1998.

[3] C. S. Kim, J. S. Park, D. Ahn, and J. B. Lim, "A novel 1-D periodic defected ground structure for planar circuits," *IEEE Microw. Guided Wave Lett.*, vol. 10, no. 4, pp. 131–133, Apr. 2000.

[4] D. Ahn, J. S. Park, C. S. Kim, J. Kim, Y. Qian, and T. Itoh, "A design of the low-pass filter using the novel microstrip defected ground structure," *IEEE Trans. Microw. Theory Tech.*, vol. 49, no. 1, pp. 86–93, Jan. 2001.

[5] J.-S. Lim, C.-S. Kim, Y.-T. Lee, D. Ahn, and S. Nam, "A spiral-shaped defected ground structure for coplanar waveguide," *IEEE Microw. Wireless Compon. Lett.*, vol. 12, no. 9, pp. 330–332, Sep. 2002.

[6] A. M. E. Safwat, F. Podevin, P. Ferrari, and A. Vilcot, "Tunable bandstop defected ground structure resonator using reconfigurable dumbbell-shaped coplanar waveguide," *IEEE Microw. Theory Tech.*, vol. 54, no. 9, pp. 3559–3564, Sep. 2006.

[7] M. F. Karim, A.-Q. Liu, A. Alphones, and A. Yu, "A reconfigurable micromachined switching filter using periodic structures," *IEEE Microw. Theory Tech.*, vol. 55, no. 6, pp. 1154–1162, Jun. 2007.

[8] M. F. Karim, A. Q. Liu, A. Alphones, and A. B. Yu, "A novel reconfigurable filter using periodic structures," in *IEEE MTT-S Int. Microw. Symp. Dig.*, Jun. 2006, pp. 943–946.

[9] K. Entesari, K. Obeidat, A. R. Brown, and G. M. Rebeiz, "A 25-75-MHz RFMEMS tunable filter," *IEEE Microw. Theory Tech.*, vol. 55, no. 15, pp. 2399–2405, Nov. 2007.

[10] K. Entesari and G. M. Rebeiz, "A differential 4-bit 6.5-10-GHzRF MEMS tunable filter," *IEEE Microw. Theory Tech.*, vol. 53, no. 3, pp. 1103–1110, Mar. 2005.

[11] S.-J. Park, I. Reines, C. Patel, and G. M. Rebeiz, "A differential 4-bit 6.5-10-GHzRF MEMS tunable filter," *IEEE Microw. Theory Tech.*, vol. 58, no. 2, pp. 381–389, Mar. 2010.

[12] G. M. Rebeiz, *RF MEMS: Theory, Design, and Technology*. New York, NY, USA: Wiley, 2003.

[13] N. Zhang, Z. Deng, C. Shu, and H. Wang, "Analyse and design a tunable band-pass filter employing RF MEMS capacitors," *IEEE Electron Device Lett.*, vol. 32, no. 10, pp. 1460–1462, Oct. 2011.

[14] K. Entesari and G. M. Rebeiz, "A differential 4-bit 6.5-10-GHz RF MEMS tunable filter," *Microw. Theory Tech.*, vol. 53, no. 3, pp. 1103–1110, Mar. 2005.

[15] I. Reines, S.-J. Park, and G. M. Rebeiz, "Compact low-loss tunable X-band band stop filter with miniature RF MEMS switches," *IEEE Trans. Microw. Theory Tech.*, vol. 58, no. 7, pp. 1887–1895, Jul. 2010.

[16] G. M. Rebeiz, K. Entesari, I. C. Reines, S.-J. Park, M. A. El-Tanani, A. Grichener, and A. R. Brown, "Tuning in RF MEMS," *IEEE Microw. Mag.*, vol. 10, no. 6, pp. 55–72, Oct. 2009.

[17] H. T. Kim, J. H. Park, Y. K. Kim, and Y. Kwon, "Millimeter wave micro machined tunable filters," in *IEEE MTT-S Dig. Int. Microw. Symp. Dig.*, vol. 3. Jun. 1999, pp. 1235–1238.

[18] H.-T. Kim, J.-H. Park, Y.-K. Kim, and Y. Kwon, "Low-loss and compact-band MEMS-based analog tunable bandpass filters," *IEEE Microw. Wireless Compon. Lett.*, vol. 12, no. 11, pp. 432–434, Nov. 2002.

[19] M. Karim, A. Lui, A. Alphones, and A. Yu, "A tunable band stop filter via the capacitance change of micromachined switches," *J. Micromech. Microeng.*, vol. 16, no. 4,, pp. 851–861, 2006.

[20] A. Abbaspour-Tamijani, L. Dussopt, and G. M. Rebeiz, "Miniature and tunable filters using MEMS capacitors," *IEEE Trans. Microw. Theory Tech.*, vol. 51, no. 7, pp. 1878–1885, Jul. 2003.

[21] S. Fouladi, W. D. Yan, and R. R. Mansour, "Microwave tunable bandpass filter with MEMS thermal actuators," in *Proc. 3rd Eur. Microw. Integr. Circuits Conf.*, Oct. 2008, pp. 482–485.

[22] M. Fernández-Bolanos, C. Dehollain, P. Nicole, and A. M. Ionescu, "Tunable band-stop filter based on single RF MEMS capacitive shunt switch with meander arm inductance," *Solid-State Electron. J.*, vol. 54, no. 9, pp. 1033–1040, 2010.

[23] H. S. Lee, D.-H. Choi, and J.-B. Yoon, "MEMS-based tunable LC band-stop filter withan ultra-wide continuous tuning range," *IEEE Microw. Wireless Compon. Lett.*, vol. 19, no. 11, pp. 710–712, Nov. 2009.

[24] Z. L. Deng, N. B. Zhang, and J.-M. Huang, "A tunable ultra-wideband band-stop filter based on EBG structures using MEMS technology," in *Proc. Mech. Autom. Int. Conf.*, Aug. 2009, pp. 3579–3583.

[25] T. Yang, M. Tamura, and T. Itoh, "Compact hybrid resonator with series and shunt resonances used in miniaturized filters and balun filters," *IEEE Microw. Theory Tech.*, vol. 58, no. 2, pp. 390–402, Feb. 2010.

[26] I. Bahl, *Lumped Elements for RF and Microwave Circuits*. Boston, MA, USA: Artech House, 2003, pp. 230–235.

[27] N. Zhang and Z. Deng, "Method to design the microwave band-stop filter based on CPW," *Electron. Lett.*, vol. 47, pp. 450–451, Mar. 2011.

[28] R. J. Roark and W. C. Young, *Formulas for Stress and Strain*, 6th ed. New York, NY, USA: McGraw-Hill, 1989.

[29] V. L. Rabinov, R. J. Gupta, and S. D. Senturia, "The effect of release etch-holes on the electromechanical behavior of MEMS structures," in *Proc. Int. Conf. Solid-State Sensors Actuat.*, Jun. 1997, pp. 1125–1128.

[30] (2013). *Source: WebElements* [Online]. Available: http://www.webelements.com/

[31] J.-S. Lim, C.-S. Kim, Y.-T. Lee, D. Ahn, and S. Nam, "A spiral-shaped defected ground structure for coplanar waveguide," *IEEE Microw. Wireless Compon. Lett.*, vol. 12, no. 9, pp. 330–333, Sep. 2002.

[32] A. B. Yu, A. Q. Liu, Q. X. Zhang, A. Alphones, L. Zhu, and S. A. Peter, "Improvement of isolation for RF MEMS capacitive shunt switch via membrane planarization," *Sens. Actuators A, Phys.*, vol. 19, pp. 206–213, Jan. 2005.

[33] A. B. Yu, A. Q. Liu, Q. X. Zhang, and H. M. Hosseini, "Effects of surface roughness on electromagnetic characteristics of capacitive switches," *J. Micromech. Microeng.*, vol. 16, pp. 2157–2166, Jul. 2006.

[34] A. B. Yu, A. Q. Liu, Q. X. Zhang, A. Alphones, and H. M. Hosseini, "Micromachined DC contact capacitive switch on low-resistivity silicon substrate," *Sens. Actuators A, Phys.*, vol. 127, pp. 24–30, Jan. 2006.

[35] J. Perruisseau-Carrier, R. Fritschi, P. Crespo-Valero, and A. K. Skrivervik, "Modeling of periodic distributed MEMS, application to the design of variable true-time delay lines," *IEEE Microw. Theory Tech.*, vol. 54, no. 1, pp. 383–392, Jun. 2005.

[36] J.-M. Huang, H. Z. Zhu, K. Han, and H. Guo, "A novel X-band broadband band-stop filter with sharp cut-off frequency using EBG dual-ear structures," *Micow. Opt. Technol. Lett.*, vol. 53, no. 7, pp. 1671–1674, 2011.

[37] Z. Brito-Brito, I. Llamas-Garro, G. Navarro-Muñoz, J. Perruisseau-Carrier, L. Pradell, F. Giacomozzi, and F. Colpo, "Precise frequency and bandwidth control of switchable microstrip bandpass filters using diode and MEMS technologies," *IET Microw. Antennas Propag.*, vol. 6, pp. 713–719, Apr. 2012.

[38] H. W. Liu, T. Yoshimasu, and L. L. Sun, "CPW bandstop filter using periodically loaded slot resonators," *Electronics Lett.*, vol. 42, no. 6, pp. 352–353, 2006.

Naibo Zhang received the Ph.D. degree from the Beijing University of Posts and Telecommunications, Beijing, China, in 2012.

His current research interests include radio frequency (RF) devices, especially RF microelectromechanical systems tunable filters.

Zhongliang Deng (M'10) received the Ph.D. degree from Tsinghua University, Beijing, China, in 1994.

He is currently a Professor of electrical engineering with the Beijing University of Posts and Telecommunications, Beijing.

Fan Sen is currently pursuing the Ph.D. degree with the Beijing University of Posts and Telecommunications, Beijing, China.

His current research interests include radio frequency microelectromechanical systems devices.